

Article citation info:

Bai R, Wang H, Sun W, Shi Y, Fault diagnosis method for rotating machinery based on SEDenseNet and Gramian Angular Field, *Eksploracja i Niezawodność – Maintenance and Reliability* 2024; 26(4) <http://doi.org/10.17531/ein/191445>

## Fault diagnosis method for rotating machinery based on SEDenseNet and Gramian Angular Field

Indexed by:



Ruoyang Bai<sup>a</sup>, Hongwei Wang<sup>a,\*</sup>, Wenlei Sun<sup>a</sup>, Yuxin Shi<sup>a</sup>

<sup>a</sup> School of Mechanical Engineering, Xinjiang University, China

### Highlights

- Utilizing the GAF coding method enables the representation of low-dimensional signal features within high-dimensional nonlinear data.
- The incorporation of the SE attention mechanism into the DenseNet model facilitates enhanced feature transfer and reuse.
- The diagnostic accuracies for the three datasets achieved were 100%, 100%, and 99.85%, respectively.

### Abstract

The fault diagnosis in rotating machinery is crucial for ensuring the safe and dependable operation of intricate mechanical systems. Addressing the limitations inherent in traditional deep learning approaches concerning extended time sequence encoding and subpar generalization capability is paramount. The study utilizes the Gramian Angular Field (GAF) and Squeeze and Excitation (SE) attention mechanisms to alleviate these constraints. GAF enhances feature extraction by emphasizing the angular relationships among adjacent signal points to uncover latent fault characteristics. Simultaneously, through the integration of SE with DenseNet architecture, the network facilitates global information exchange and improves multi-scale fusion, thereby enhancing the precise identification of fault type and location within the signal. Experiments conducted on two datasets achieved accuracies of 100% and 99.85%, respectively, outperforming other methods and models, thereby validating the effectiveness of this study.

### Keywords

rotating machinery, fault diagnosis, Gramian Angular Field, SEDenseNet

This is an open access article under the CC BY license (<https://creativecommons.org/licenses/by/4.0/>)

### 1. Introduction

In the industrial sector, there is a substantial presence of rotating machinery. However, these machines often face various failures during engineering practice, which can result in significant damage, as well as severe injury or even loss of life. Many faults exhibit numerous ambiguous features. Therefore, conducting research on feature extraction and analysis methods for fault diagnosis of rotating machinery holds immense importance 1.

Traditional fault diagnosis methods based on expert systems heavily rely on the expert's empirical knowledge, leading to high manual labor intensity and low accuracy in real engineering environments 2. These methods are based on mechanical fault mechanisms, signal characteristics, or feature

extraction. Traditional fault diagnosis using expert systems relies on experts' practical experience and professional knowledge of rotating machinery, making it difficult to carry out efficient fault diagnosis 3. Machine learning-based fault diagnosis is a data-driven method that utilizes machine learning techniques to automate the diagnosis of faults in equipment or systems 4. The model is trained with historical data and applied to real-time data to determine the type and location of faults. Ye et al. 5 used variational modal decomposition to decompose the original mechanical vibration signal into multiple intrinsic modal functions, constructed multidimensional feature vectors of the signal through multiscale permutation entropy, and

(\*) Corresponding author.

E-mail addresses:

R. Bai (ORCID: 0009-0005-3831-9716) [ruoyangbai@163.com](mailto:ruoyangbai@163.com), H. Wang (ORCID: 0000-0002-8598-2343) [wanghongwei\\_xju](mailto:wanghongwei_xju), W. Sun (ORCID: 0000-0003-2287-9514) [sunwenxj@163.com](mailto:sunwenxj@163.com), Y. Shi (ORCID: 0009-0008-1094-9769) [shiyuxinpayne@163.com](mailto:shiyuxinpayne@163.com),

inputted the multidimensional vectors into a particle swarm optimization-based support vector machine classification model to achieve the diagnosis of fault diagnosis of rolling bearings. Liu et al. 6 proposed a method based on twin prototype networks with noisy label self-correction to address fault diagnosis for wind turbine gearboxes with noisy labels. Guo et al. 7 proposed a measure of the intensity of periodic pulses in the signal, cyclic kurtosis entropy, to address the problem of rotating machinery that may lead to failure of fault diagnosis techniques in the presence of strong noise disturbances or composite fault coupling phenomena. The algorithm utilizes the entropy value to calculate all delayed periodic kurtosis, overcoming the shortcomings of poor adaptive ability of kurtosis and obtaining a more stable value, resulting in enhanced fault feature extraction of rotating machinery under stationary operating conditions. Su et al. 8 proposed a novel intelligent fault diagnosis model based on singular value manifold features, optimized support vector machines and multi-sensor information fusion. Li et al. 9 tackled the issue of frequency distortion caused by strong noise or dense frequencies in rotating machinery by mapping the signal into a new pseudo-temporal domain to eliminate non-smoothness in the basis of the rotating machinery mechanism. They also addressed the impact of velocity variations or acceleration fluctuations at complex and dense frequencies on fault diagnosis. Li et al. 10 proposed an interpretable wavelet packet kernel-constrained convolutional network for noise robust fault diagnosis, which demonstrated superior robustness and noise immunity compared to other models. Aasi et al. 11 established a setup specifically designed for condition monitoring of angular contact bearings using acoustic emission sensors. During the experimentation process, acoustic emission signals were collected from bearings containing defects, with a focus on analyzing and recording defects occurring on the inner or outer rings of the bearings. By screening and conducting a detailed analysis of several common time-domain features, the results revealed the applicability of these features in diagnosing the condition of the bearings. Notably, the clearance factor demonstrated significant effectiveness in detecting small-sized defects, and the sixth-order central moment was particularly adept at identifying larger defects. This research provides an efficient technical method for the industrial application of

rolling bearing condition monitoring and fault detection.

The implementation of machine learning has facilitated certain advancements in the field of fault diagnosis 12. However, due to its shallow architecture, machine learning often struggles with obtaining high-dimensional and invisible characterizations 13. In the realm of big data, deep learning-based algorithms have emerged as a prominent area of focus for fault diagnosis. These algorithms can learn fault features from raw fault signals without relying on expert experience or manual extraction, making deep learning-based fault diagnosis methods a popular research direction among scholars in recent years. Zhang et al. 14 proposed a Bayesian augmented convolutional neural network, which focuses on capturing the time dependence of the signals in non-stationary relationships collected from raw fault signals and achieves impressive results in the fault diagnosis of large-scale low-speed wind turbine bearings. Wang et al. 15 proposed an adaptive denoising convolutional neural network, which integrates an adaptive denoising unit to remove noise while retaining sensitive fault features, eliminating the need for manual denoising function setting and achieving superior fault diagnosis performance in noisy environments. Wang et al. 16 proposed a fast fault diagnosis method based on the swarm decomposition algorithm, the improved multi-scale reverse discrete entropy algorithm, and bidirectional long-term memory network for gear transmission systems, achieving high accuracy and stability in fault signal classification. Chen et al. 17 proposed a nonlinear system identification strategy based on deep migration learning domain adversarial neural network, achieving high identification accuracy in 16 operating conditions of helicopter transmission systems. Cheng et al. 18 proposed a wavelet transform-local two-stage convolutional neural network fault diagnostic method, in which vibration signals from bearings are passed through a wavelet transform and then separately input to a local two-cross convolutional neural network to diagnose rotating machinery. Since machinery failures do not exhibit only one characteristic, methods that fuse multiple source signals into a neural network for fault diagnosis have been proposed. Wang et al. 19 proposed a multi-modal sensor fusion method, using acceleration sensors and acoustic sensors to collect vibration and acoustic signals respectively and feeding the collected signals into a constructed binary convolutional neural network to carry out fault diagnosis.

Luo et al. 20 proposed an intelligent motor bearing early fault diagnosis algorithm based on Wasserstein GAN Meta learning, and verified its superiority compared with existing algorithms.

It is widely recognized that Convolutional Neural Networks (CNNs) have shown excellent performance in fault diagnosis and prediction tasks. CNNs are primarily used for 2D image processing, but they have also been successfully applied to equipment fault diagnosis and prediction due to their strong feature learning ability and fault tolerance in complex environments and confusing knowledge rules. There are two main strategies for using CNNs for rotating machinery fault diagnosis: one is to use a 1D-CNN model and input one-dimensional mechanical signals into the network to diagnose faults; the other is to convert one-dimensional mechanical signals into two-dimensional images and input them into the network. Xia et al. 21 combined the raw data collected by multiple sensors into a 2D matrix and input the raw data into the CNN in 2D form to achieve end-to-end feature learning. Chen et al. 22 proposed a method of combining cyclic spectral Cscoh 2D maps with CNNs using double Fourier transform to estimate vibration signal 2D Cscoh maps and reveal valuable health state information. Xiong et al. 23 proposed a vibration signal for fault diagnosis using mutual dimensionless similarity Gram matrix data preprocessing and feeding the processed feature maps into the CNN for diagnosis. Bai et al. 24 proposed a new spectral Markov transfer field algorithm, which constructs a first-order Markov transfer matrix of frequency domain signals to represent the spectral characteristics of vibration signals as an image and shows effectiveness in comprehensively characterizing composite fault features. He et al. 25 proposed a multi-sensor data fusion method that integrates multivariate data into pixel matrices and feeds these matrices into a two-scale residual network for fault diagnosis. Fan et al. 26 proposed a graph generation method to generate correlation diagrams from table data and feed these diagrams into neural networks for HVAC system fault diagnosis. Chang et al. 27 initially transformed the battery voltage signal into a time-frequency representation through continuous wavelet transform following variational modal decomposition. Subsequently, they utilized image entropy to decipher the parameters of the battery malfunction for fault diagnosis.

The utilization of attention mechanisms in intelligent fault

diagnosis enhances the accuracy of classification by selectively focusing on relevant features and suppressing irrelevant information, thereby greatly improving efficiency. Wang et al. 28 applied Empirical Mode Decomposition to preprocess the original signal, incorporated a multi-head attention mechanism into the graph neural network, and achieved notable performance in bearing diagnosis. Tong et al. 29 proposed a CNN model utilizing multi-sensor information fusion and coordinated attention, resulting in a lightweight convolutional neural network with integrated attention mechanism, known as ACNN. Xia et al. 30 introduced a hierarchical attention-based method for multi-source data fusion fault diagnosis in autonomous underwater vehicles. The method employs an encoder-decoder network, a fusion network stacked with encoders, and an attention mechanism to diagnose faults. Validation of the method was conducted using monitoring data from the "Submarine Dragon II" underwater robot during sea trials in the South China Sea, which demonstrated its effectiveness.

Despite the advancements made by the aforementioned methods in fault diagnosis, the realm of mechanical fault diagnosis confronts persistent challenges in real-world operational scenarios. Rotating mechanical equipment typically operates under fluctuating load conditions, resulting in dynamic alterations in fault information. Moreover, the vibration signals captured by sensors often exhibit high levels of complexity, coupling, and uncertainty. Conventional deep learning models lack the adaptability to dynamically extract fault features in accordance with specific requirements, thereby resulting in inadequate generalization of the models for practical engineering applications.

To address the inherent limitations of traditional deep learning methods in expanding time series encoding and generalization capabilities, as well as to facilitate global information exchange in fault diagnosis models and enhance multi-scale feature fusion, this study has designed a fault diagnosis model based on GAF encoding technology and SEDenseNet . This approach aims to achieve precise identification of fault types and locations within signals. This method is employed to detect common fault conditions in bearings and gears within rotating machinery, thereby preventing losses in engineering projects. The design concept

entails merging deep learning and signal processing methodologies to enhance the efficacy of fault diagnostic detection. This is achieved by incorporating the GAF coding technique to capture the fault characteristics of signals and integrating it into the deep learning framework. The fault characteristics embedded within vibration signals, encompassing multivariate time domain information, are extracted utilizing the angular parsing mechanism of GAF coding, thereby enhancing the feature representation. Subsequently, the resultant feature maps are processed through the SE Attention module and DenseNet module to recalibrate the feature maps. Leveraging learnable weight parameters, the model dynamically selects and accentuates pivotal information within the feature maps, thus augmenting the model's capability to discern fault features. The efficacy of the proposed methodology is validated across three dataset, affirming its robust performance.

## 2. Gramian Angular Field

The GAF image encoding method maintains the time dependence of the signal [31], with the time sequence information increasing as the location moves from the upper left corner to the lower right corner, ensuring that no information is lost within the signal. The main process for constructing a GAF is as follows:

First, given the time series  $X = \{x_1, x_2, \dots, x_n\}$  of  $n$  values of a vibration signal, rescale  $X$  so that all signal values fall within the interval  $[0, 1]$ , and perform normalization processing on  $X$  to obtain  $\tilde{x}_i$ ; then encode the signal values into cosine angles using the following equation and encode the timestamps into radii to represent the rescaled time series  $X$  in polar coordinates.

$$\begin{cases} \phi = \arccos(\tilde{x}_i), -1 \leq \tilde{x}_i \leq 1, \tilde{x}_i \in \tilde{X} \\ r = \frac{t_i}{N}, t_i \in N \end{cases} \quad (1)$$

In the above equation, it is the timestamp and  $N$  is the constant used to regularize the span of the polar coordinate system. Since  $\cos(\phi)$  is monotonic when  $\phi \in [0, \pi]$ , the above equation is bijective.

Angular perspective is utilized to consider the triangular sum or triangular difference coming between each point, thus identifying temporal correlations in different time intervals. Gramian Angular Summation Field(GASF) and Gramian Angular Difference Field(GADF) are defined as follows:

$$\begin{aligned} GASF &= [\cos(\phi_i + \phi_j)] \\ &= \tilde{X}' \cdot \tilde{X} - \sqrt{I - \tilde{X}^2} \cdot \sqrt{I - \tilde{X}^2} \end{aligned} \quad (2)$$

$$G_S = \begin{pmatrix} \cos(\phi_1 + \phi_1) & \cdots & \cos(\phi_1 + \phi_n) \\ \vdots & \ddots & \vdots \\ \cos(\phi_n + \phi_1) & \cdots & \cos(\phi_n + \phi_n) \end{pmatrix} \quad (3)$$

$$\begin{aligned} GADF &= [\sin(\phi_i - \phi_j)] \\ &= \sqrt{I - \tilde{X}^2} \cdot \tilde{X} - \tilde{X}' \cdot \sqrt{I - \tilde{X}^2} \end{aligned} \quad (4)$$

$$G_D = \begin{pmatrix} \sin(\phi_1 - \phi_1) & \cdots & \sin(\phi_1 - \phi_n) \\ \vdots & \ddots & \vdots \\ \sin(\phi_n - \phi_1) & \cdots & \sin(\phi_n - \phi_n) \end{pmatrix} \quad (5)$$

Where  $I$  is the unit row vector  $[1, 1, \dots, 1]$ . One-dimensional time series can be transformed into quasi-Gramian matrix by the above transformation. Due to the large size of the  $n \times n$  Gramian matrix, Piecewise Aggregate Approximation [32] is used to smooth the time series while maintaining the trend of the signal. The GAF generation process is shown in Fig. 1. Every pixel in the GAF 2D image corresponds to the magnitude of the value in the corresponding position of the proposed Gramian matrix. Given that GASF and GADF compute the angle between neighboring points of the temporal signal in distinct manners, the resulting 2D images exhibit disparities.

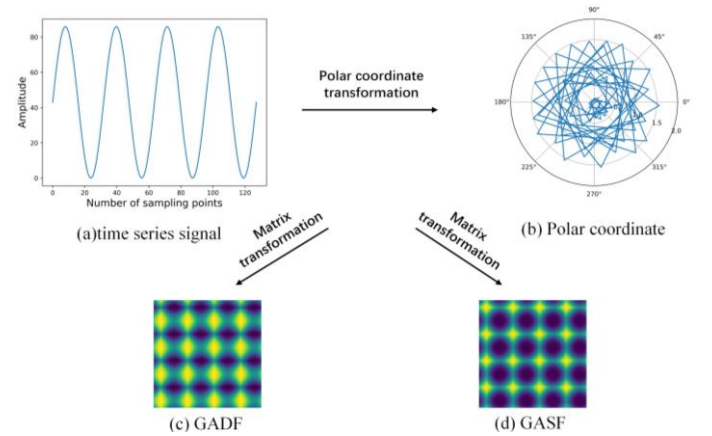


Fig. 1. Schematic diagram of GAF generation.

## 3. SEDenseNet components

### A DenseNet

ResNet allows for deeper training by establishing "shortcuts" (skip connections) between front and back layers. Conversely, DenseNet establishes dense connections between all previous layers and those behind them. DenseNet solves gradient vanishing issues in deep CNNs and enhances feature transfer and reuse [33]. This dense connectivity regularization can reduce

overfitting in small dataset to some extent. At its core, the dense connection mechanism is the foundation of DenseNet, which is

illustrated in Fig. 2.

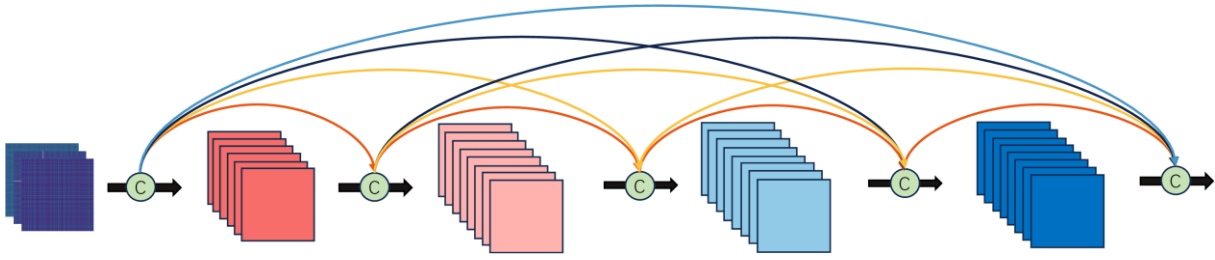


Fig. 2. Dense connection mechanism.

A dense connection block makes any layer directly connected to all subsequent layers, and the  $n$ th layer receives the feature maps  $x_0, x_1, \dots, x_{L-1}$  as input:

$$x_L = H_L([x_0, x_1, \dots, x_{L-1}]) \quad (6)$$

Where  $[x_0, x_1, \dots, x_{L-1}]$  are the connections of the feature maps generated at layers 0, 1, ..., L-1 layers of the resulting feature maps are connected, and  $H_L()$  is a nonlinear transformation

composite function of three consecutive operations, including batch normalization (BN), rectified linear unit (ReLU),  $3 \times 3$  convolutional (Conv) and average pooling. Dense connected blocks are alternately connected in series with the transition layer to form the DenseNet module. The structure of the transition layer is shown in Fig. 3.

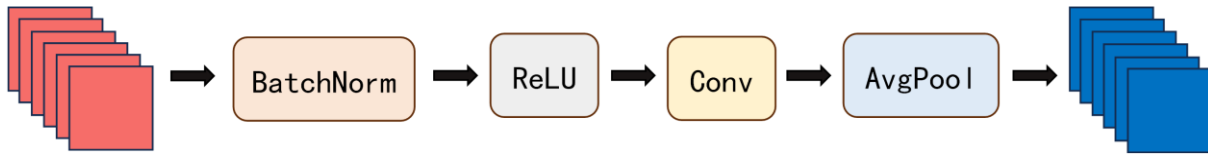


Fig. 3. Transitional layers.

### B Squeeze-and-Excite Attention Mechanism

The Squeeze-and-Excitation attention mechanism is originated from SENet 34. SE attention module introduces a weight matrix

to assign different weights to different locations in the image from the perspective of channel domain, so as to obtain more important feature information from different channels. The structure is shown in Fig. 4.

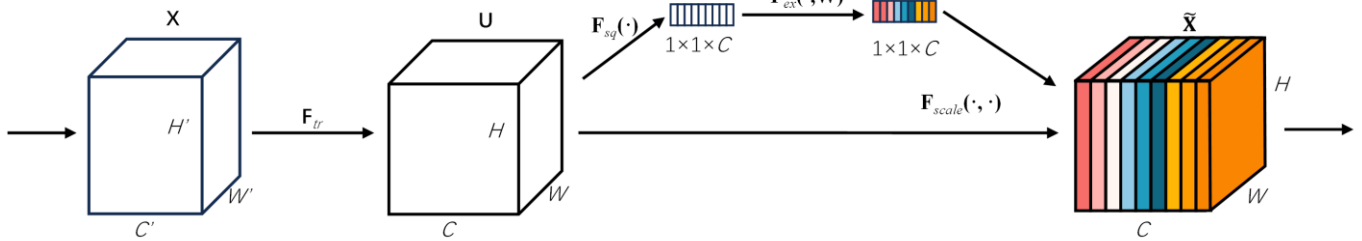


Fig. 4. Squeeze and Excitation module.

SE attention mechanism implementation steps are as follows:

Transformation( $F_{tr}$ ): Enter a feature map  $X$  and generate a feature map  $X$  after  $F_{tr}$  operations.

Squeeze( $F_{sq}()$ ): The feature graph is globally average pooling to generate a vector of  $1 \times 1 \times C$ , and each channel is represented by a numerical value, thus realizing the global information of  $U$  is low-dimensional, so that a numerical value has the global sensitivity field of the channel.

$$z_c = F_{sq}(u_c) = \frac{1}{H \times W} \sum_{i=1}^H \sum_{j=1}^W u_c(i, j) \quad (7)$$

Excitation( $F_{ex}$ ): This operation is realized by two fully connected layers (FC), the weights ( $W$ ) obtained from learning to indicate the importance of the features, the  $z$  obtained in the previous step is processed by  $W_1$  and  $W_2$  of the two fully connected layers (FC) to obtain the desired channel weight value  $s$ . After two fully connected layers,  $s$  to indicate the weight information of different channels.

$$s = F_{ex}(z, W) = \sigma(g(z, W)) = \sigma(W_2 \delta(W_1 z)) \quad (8)$$

Scale( $F_{scale}$ ): Assign the weight vector  $s$  generated in the previous step to the feature map  $U$  to obtain the feature map  $X_{\sim}$ , whose size is the same as the feature map  $U$ . The SE attention module does not change the size of the feature map.

$$\tilde{x}_c = F_{scale}(u_c, s_c) = s_c u_c \quad (9)$$

By multiplying the generated feature vector  $s(1 \times 1 \times C)$  with the feature map  $U(H \times W \times C)$ , even if the  $H \times W$  individual values of each channel in the feature map  $U$  are multiplied by the weights of the corresponding channel of  $s$ , so that each channel dimension realizes the calibration of the feature.

#### 4. Experimental data and model

This section presents two types of experimental data and describes the experimental model. The experiments utilize Case Western Reserve University (CWRU) motor bearing fault diagnosis dataset, as well as the bearing fault data and gearbox

fault data collected by Wind Turbine Drivetrain Simulator Fault Diagnosis Comprehensive Experimental Platform. These dataset are used to validate the proposed rotating machinery fault diagnosis method based on SEDenseNet and Gramian angular field.

#### A Case 1: Case Western Reserve University Bearing Dataset

The experimental data for Case 1 was obtained from the motor bearing troubleshooting testbed at Case Western Reserve University 35. The platform in Fig. 5, which includes a 2-hp electric motor, torque transducer, power test meter, and electronic controller (not shown), serves as the experimental setup. The data was acquired at the drive end of the bearing model SK6205, with a sampling frequency of 12 kHz, bearing speed of 1797 r/min, and under no load conditions.

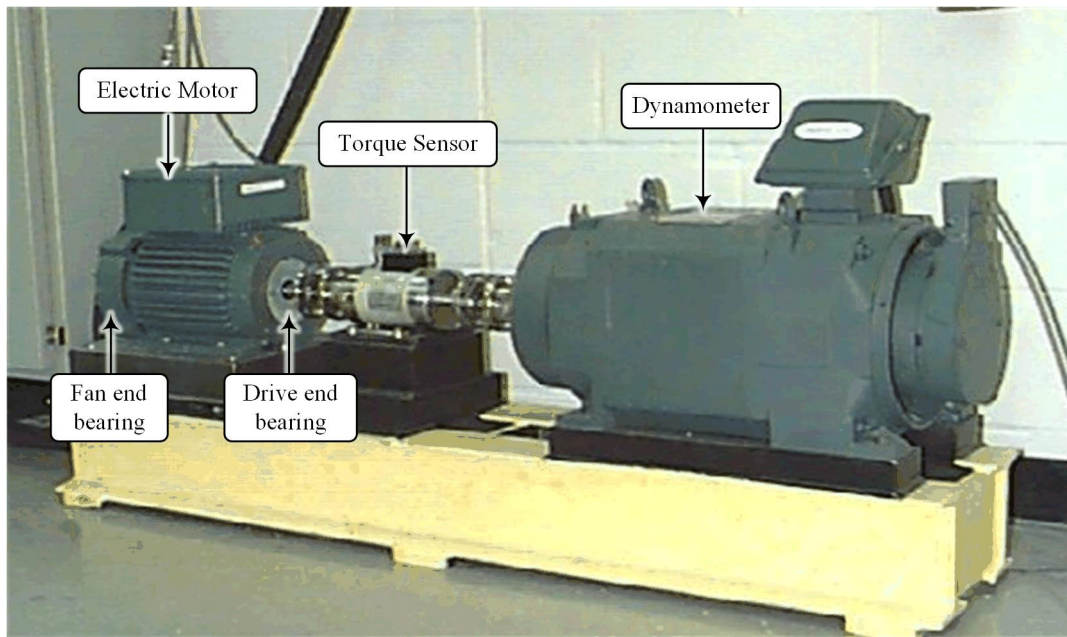


Fig. 5. CWRU experimental setup.

The bearing dataset comprises four health conditions: normal state (N), inner race fault (IR), outer race fault (OR), and ball fault (Ball). The data was collected from the drive-end bearing and is presented in Table 1. To augment the network model's learning and generalization capabilities, this paper employs dataset augmentation techniques to expand the dataset. Specifically, one-dimensional bearing vibration signals are oversampled using overlapping sampling, whereby there is an overlap between consecutive samples. The sampling method is

illustrated in Fig. 5, and the signal length of each sample segment, overlap step, and final total number of samples can be determined using the following formula.

$$n = \frac{N-Sl}{Sl-Ol} + 1 \quad (10)$$

Where  $N$  represents the length of a health type vibration signal;  $n$  represents the total number of samples,  $Ol$  represents the overlap step, and  $Sl$  represents the length of each sample.

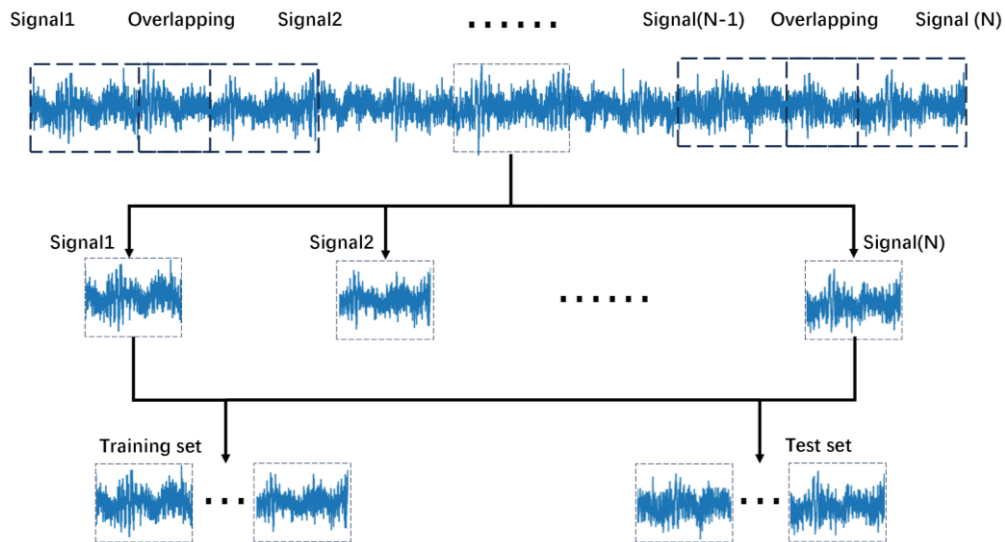


Fig. 6. Signal sample interception.

In order to make the length of each sample signal greater than the length of the signal produced by the bearing rotating for two weeks ( $12000 \times 60 / 1797$ ), the length of each section of the sample signal was selected to be 1000, the step size was 500,

and 240 samples of each type, totaling 1,680 samples for the seven types. According to the ratio of 8:2 the samples are divided into training set, test set. Where Figs 7, 8 give the GAF for the seven data transformations of Case 1.

Table 1. Details of the experimental dataset selected from the CWRU dataset.

Label	Fault type	Sample size	Fault diameter(mm)	Frequency	Speed r/min	Load	Sample length
N	Normal	240	0	12kHz	1797	0	1000
IR1	Inner Race fault	240	0.3556	12kHz	1797	0	1000
IR2	Inner Race fault	240	0.7112	12kHz	1797	0	1000
OR1	Outer Race fault	240	0.3556	12kHz	1797	0	1000
OR2	Outer Race fault	240	0.7112	12kHz	1797	0	1000
Ball1	Roller fault	240	0.3556	12kHz	1797	0	1000
Ball2	Roller fault	240	0.7112	12kHz	1797	0	1000

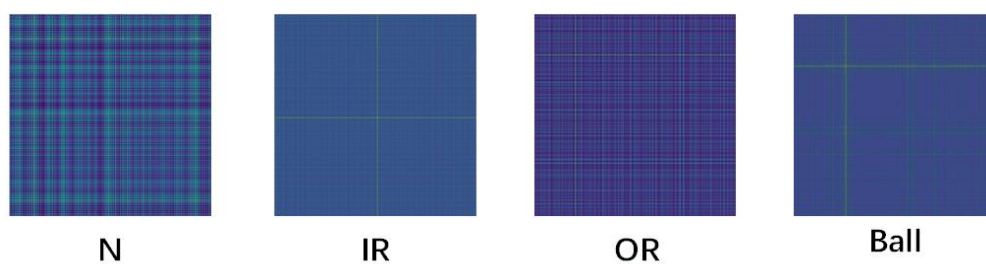


Fig. 7. GASF of CWRU bearing health status.

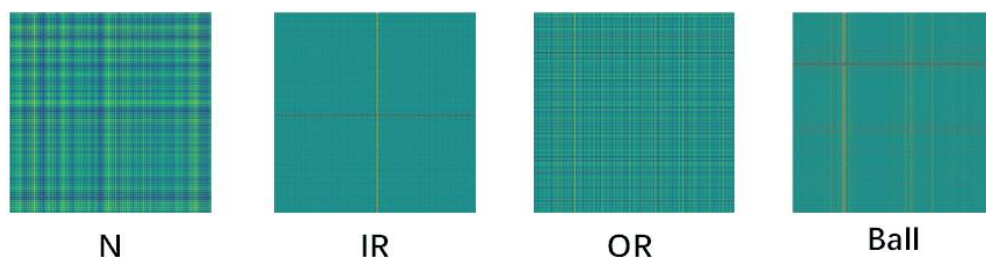


Fig. 8. GADF of CWRU bearing health status.

During the experiment, it was found that the diagnostic accuracy of these two images was not much different, so GASF with smaller storage space was selected as the input of SEDenseNet.

### B Case 2: Wind Turbine Drivetrain Simulator Dataset

The experimental data for Case 2 were obtained from the Wind Turbine Drivetrain Simulator(WTDS) Fault Diagnosis

Comprehensive Experimental Platform, which comprises a motor controller, a drive motor, a speed sensor at the drive end, a bearing housing, a parallel gearbox, a planetary gearbox, a magnetic powder brake, and an output speed sensor. The sampling frequency of the faulty acceleration signals of the bearings and gearboxes detected by the WTDS is 20480Hz, and the type of faulty bearing in question is ER-16K.

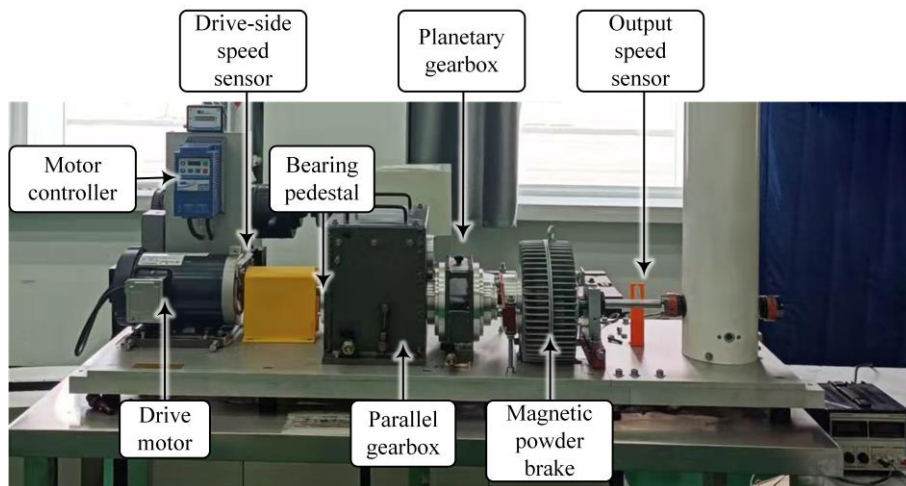


Fig. 9. WTDS experimental setup.

The bearing dataset includes the following four health types: normal condition (N), inner race fault (IR), outer race fault (OR), and ball fault (Ball), as shown in Table 2. Same as CWRU bearing data set division, in order to make each sample signal length is greater than the length of the bearing and gear rotation two weeks to produce signals ( $20480 \times 60/1500$ ), selected each

sample signal length of 2000, while making the two adjacent signal overlap length of 1000 to ensure sufficient data. The gearbox dataset consists of the following four health states: normal state (N), broken tooth (BT), tooth surface wear (TSW), and gear tooth crack (GTC), as shown in Table 3.

Table 2. Details of the experimental dataset selected from the WTDS bearing dataset.

Label	Fault type	Sample size	Load(hp)	Frequency (Hz)	Speed r/min	Sample length
N	Normal	480	0.4	20480	1500	2000
IR1	Inner Race fault	480	0.8	20480	1500	2000
IR2	Inner Race fault	480	1.2	20480	1500	2000
OR1	Outer Race fault	480	0.8	20480	1500	2000
OR2	Outer Race fault	480	1.2	20480	1500	2000
Ball1	Ball fault	480	0.8	20480	1500	2000
Ball2	Ball fault	480	1.2	20480	1500	2000

Table 3. Details of the experimental dataset selected from the WTDS gearbox dataset.

Label	Fault type	Sample size	Load(hp)	Frequency (Hz)	Speed r/min	Sample length
N	Normal	240	0.4	20480	1500	2000
TSW1	Tooth Surface Wear	240	0.8	20480	1500	2000
TSW 2	Tooth Surface Wear	240	1.2	20480	1500	2000
GTC1	Gear Tooth Crack	240	0.8	20480	1500	2000
GTC2	Gear Tooth Crack	240	1.2	20480	1500	2000
BT1	Broken Tooth	240	0.8	20480	1500	2000
BT2	Broken Tooth	240	1.2	20480	1500	2000

### C Experimental model

The present study employs a CNN model based on DenseNet to classify GADFs derived from rotating machinery vibration signals. The DenseNet169 network architecture primarily comprises of DenseBlocks and Transition layers. SEDenseNet

that retains the DenseBlock and Transition components of DenseNet while incorporating the SE attention mechanism into the feature extraction layer of DenseNet. This leads to an enhancement in the feature extraction capability of the model. The proposed methodology is illustrated in Fig. 10.

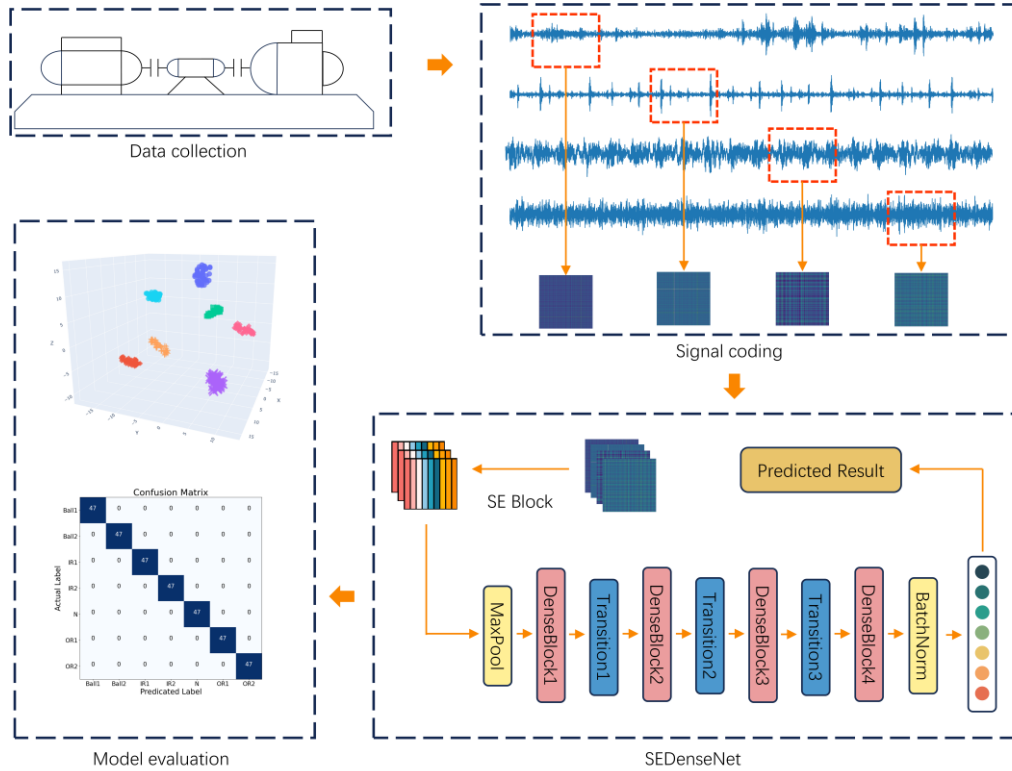


Fig. 10. Proposed fault diagnosis method for rotating machinery.

The segmented signal samples are initially transformed into a 500×500 two-dimensional image via GAF coding technique. The image is subsequently scaled to a dimension of 224×224 before being incorporated into the network model.

Following these layers, the GAF containing health status information of rotating machinery is classified, resulting in loss error and accuracy being obtained. The backpropagation of loss error is performed to optimize the network model and retrain it to minimize the gradient, thus enabling the network to be trained for 100 iterations to achieve optimal classification results.

### D Experimental platform setup

A fault diagnosis model for rotating machinery is developed using the programming language Python 3.8, running on the PyTorch deep learning framework. Development tools such as PyCharm are employed, and the code is executed in a computing environment utilizing CUDA v12.1 and an NVIDIA GeForce RTX 3060 computer graphics card. The batch

size for each feed during network training is set to 20, and the Nesterov-accelerated Adaptive Moment (Nadam) Estimation algorithm is utilized to update the network training parameters. Cross-entropy is applied to calculate the model loss. The initial learning rate is set at 0.001, and a fixed-step descent method is used to update the learning rate, which is reduced by a factor of 0.7 after every five iterations.

### 5. Experimental results and comparative analysis

This chapter further validates the superiority of the rotating machinery fault diagnosis method proposed in this paper by diagnosing the fault class types of the two dataset and comparing other network models with signal preprocessing methods.

#### A Fault diagnosis in Case 1

The vibration signals of the seven bearing health states selected in Case 1 were fed into an experimental model for training, and

as the number of iterations increased, the model continued to learn and optimize until convergence. The recognition accuracy and loss of these seven bearing health states under Case 1 are presented in Fig. 11.

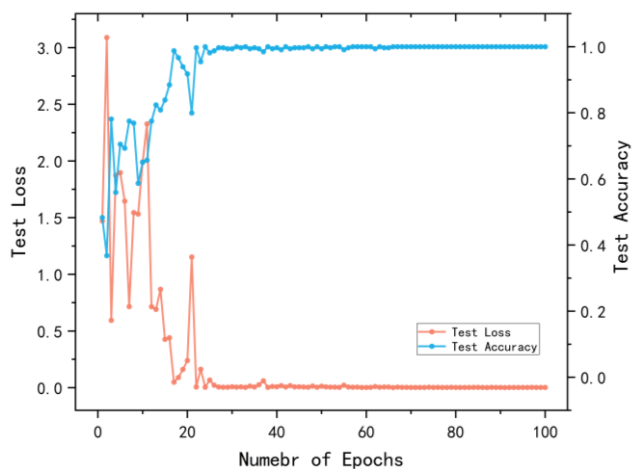


Fig. 11. Test set accuracy and loss under Case 1.

As can be observed from the figure, the model achieves

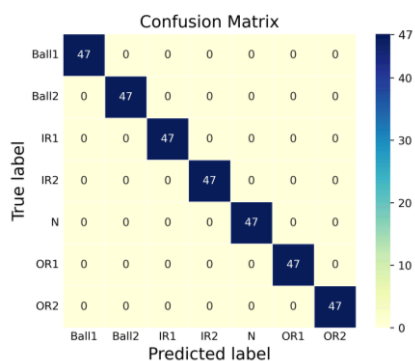


Fig.12 Confusion matrix of Case 1 data.

To assess the effectiveness of the network models proposed in this paper, a comparative analysis was conducted by comparing six different models: SEDenseNet, DenseNet, EfficientNet, ResNet50, ShuffleNet, and VGG16. The

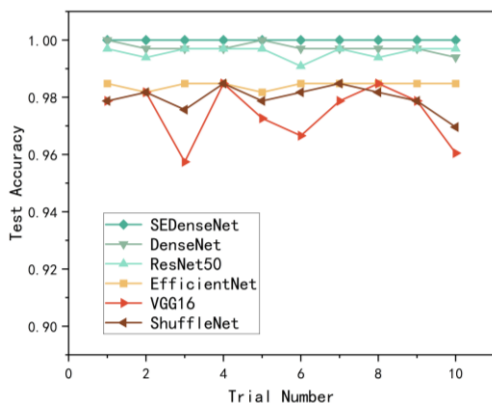


Fig. 14. 10 times accuracy of different network models for case 1

convergence at approximately 25 iterations. Thereafter, while there may be slight fluctuations in accuracy and loss, they are not significant. By the time 65 iterations have been reached, the model has fully converged and ultimately attains a perfect 100% accuracy on the test set with minimal loss.

A confusion matrix is used to evaluate the performance of a classification model in predicting the correct label for a given input. As shown in Fig. 12, the health status information in the test set of 7 are correctly classified in their corresponding positions.

t-SNE (t-distribution stochastic neighbor embedding) is a non-supervised, nonlinear dimensionality reduction algorithm that is used to visualize high-dimensional data by reducing it to two or three dimensions while preserving local features of the data. As illustrated in Fig. 13, after completing 100 rounds of training, the network model has successfully distinguished all seven health states of the bearings and no cases of misclassification have been observed.

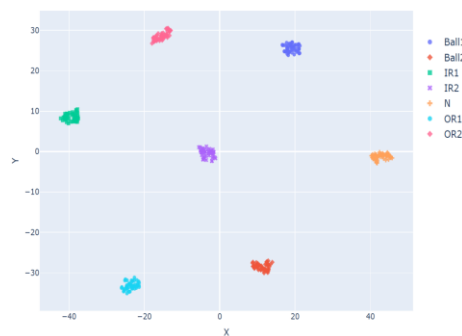


Fig.13 t-SNE of Case 1 data.

experiments were repeated for ten iterations each time, with failures during training results being excluded from the final analysis. The results are presented in Figs 14,15.

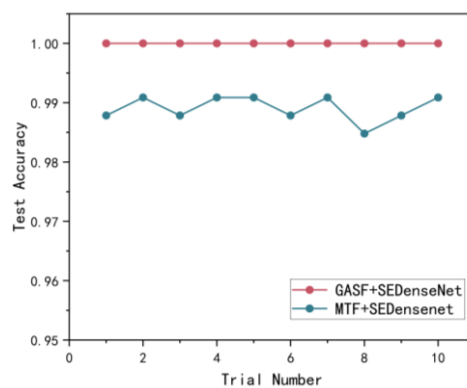


Fig. 15. Case 1 signal preprocessing method 10 times accuracy.

As can be observed from the Fig.14, the proposed network model in this paper consistently achieves 100% accuracy in recognizing bearing health information across all 10 validations. While other network models also achieve a recognition rate of over 95%, they do not guarantee correct recognition of certain samples and there remains some gaps between their performance and that of the network model proposed in this paper.

To evaluate the effectiveness of the proposed GAF coding technique for extracting health information from vibration signals, a comparison was made with the Markov Transformation Field (MTF) coding technique. Ten tests were conducted and their results were analyzed in detail as shown in Fig.15. The comparison revealed that while the MTF coding technique failed to achieve 100% accuracy in diagnosing the health status of bearings in the Case 1 dataset, it did manage to attain 98.91% accuracy when using the network model

proposed in this paper.

Table 4. Comparison of average accuracy of different network models and signal preprocessing methods.

Model	Accuracy(%)
GAF+SEDenseNet	100±0
GAF+DenseNet	99.73±0.17
GAF+ResNet50	99.57±0.21
GAF+EfficientNet	98.42±0.13
GAF+VGG16	97.45±0.98
GAF+ShuffleNet	97.96±0.45
MTF+SEDenseNet	98.91±0.21

## B Fault Diagnosis under Case 2

In this section, the health state data of bearings and gearboxes collected by the WTDS experimental platform is recognized and diagnosed. A series of evaluations of the diagnostic effects are conducted, including the recognition accuracy and loss of the WTDS bearing and gearbox dataset health state shown in Figs 16 and 17.

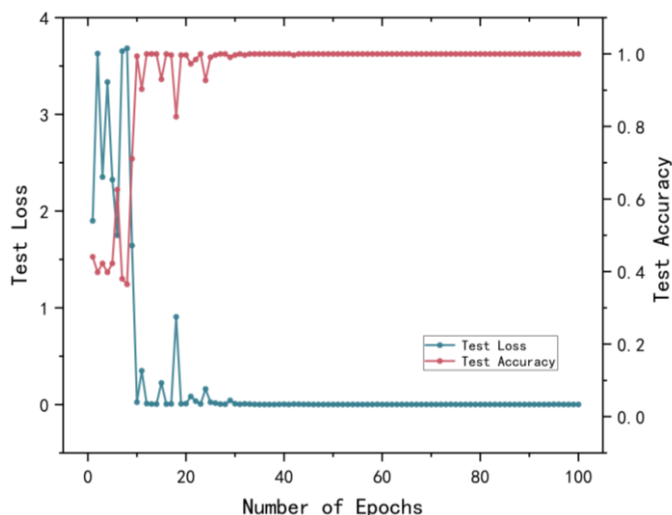


Fig. 16. Gearbox dataset accuracy and loss in Case 2.

As can be seen from the figures, the gearbox and bearing dataset of the WTDS experimental platform exhibit a gradual convergence after around 20 rounds of training. Even though there may be slight fluctuations in accuracy and loss, the magnitude of these changes is not significant. After approximately 40 rounds of training, the test set accuracy for both dataset remains consistently high, with the gearbox dataset achieving an accuracy of almost 100% and the bearing dataset achieving an accuracy of almost 99.86%. Additionally, both dataset have nearly zero loss after reaching this point of convergence.

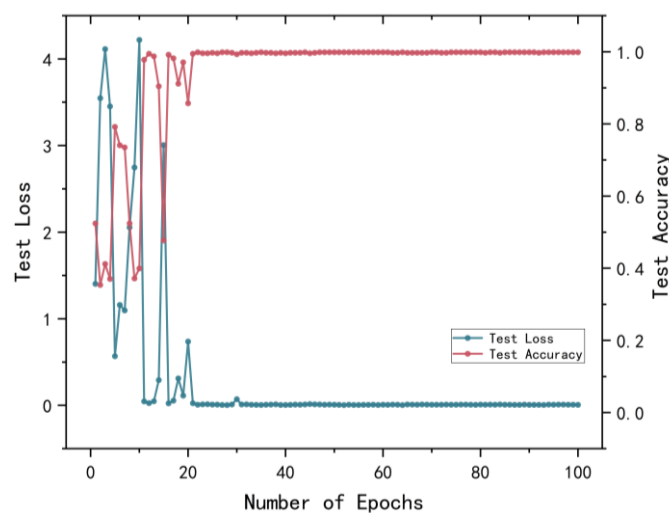


Fig. 17. Bearing dataset accuracy and loss in Case 2.

The confusion matrix in Figs. 18,19 and the t-SNE visualization in Figs. 20,21 demonstrate that all samples in the Case 2 gearbox dataset were correctly classified in the test set, while one sample of the ball fault at 0.8hp load in the test set of the Case 2 bearing dataset was incorrectly classified as the outer ring fault at 0.8hp load. The error resulted in a diagnostic accuracy of 99.86% for the bearing data test set.

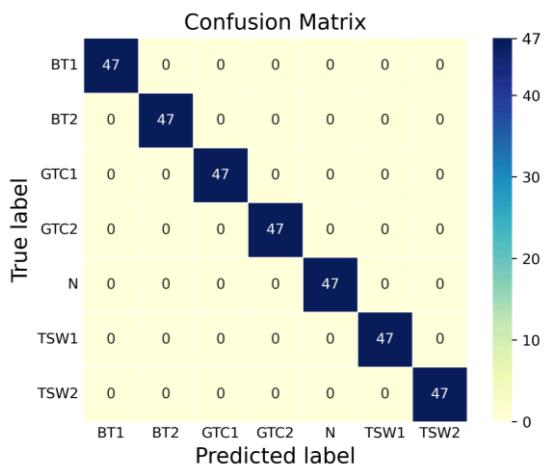


Fig. 18. Case 2 Gearbox Data Confusion Matrix.

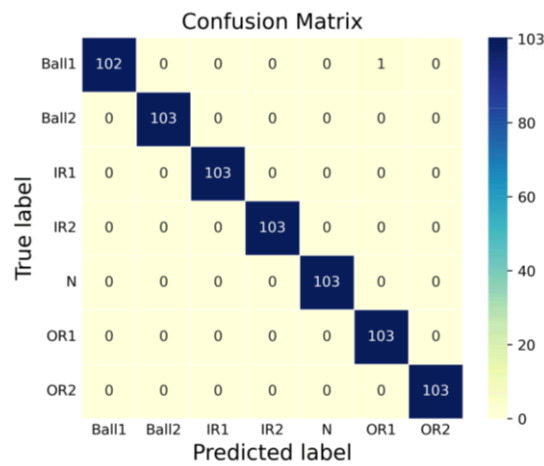


Fig. 19. Case 2 Bearing Data Confusion Matrix.

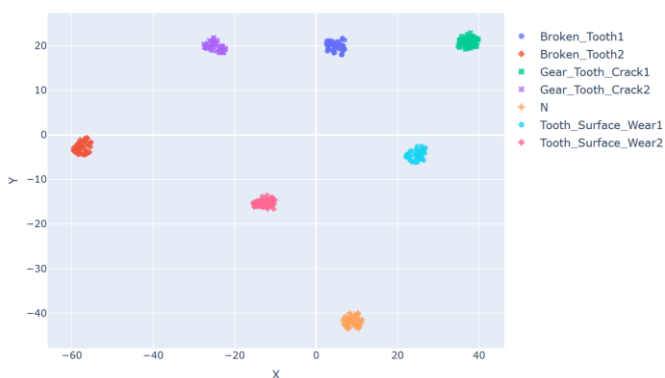


Fig. 20. Case 2 gearbox data t-SNE.

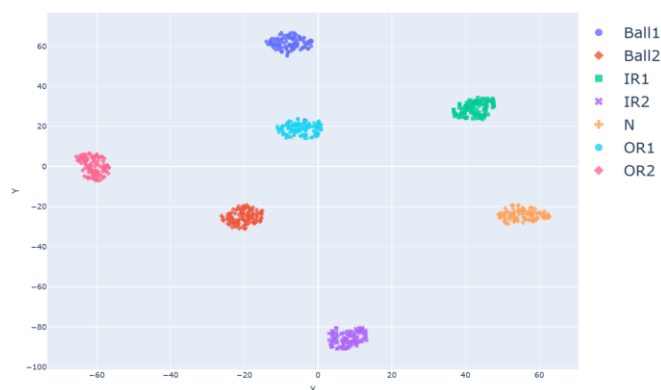
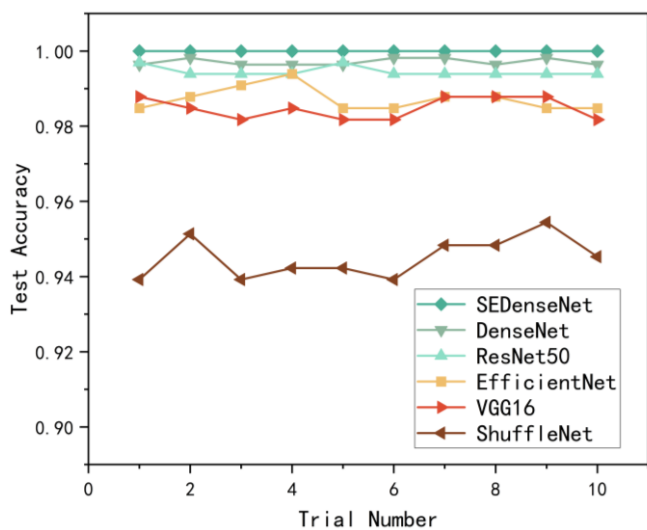


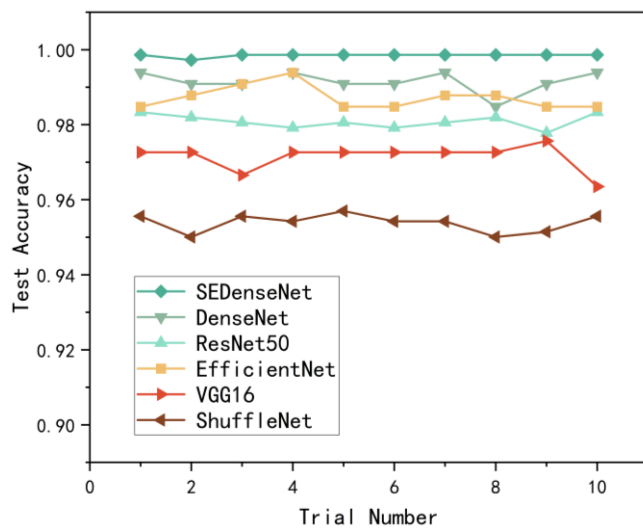
Fig. 21. Case 2 bearing data t-SNE.

Similar to the comparison experiment for the Case 1 dataset, a comparison was conducted between six network models: SEDenseNet, DenseNet, EfficientNet, ResNet50, ShuffleNet, and VGG16. Additionally, MTF coding techniques were

compared. Each method was tested 10 times (excluding any training failures) and the results were analyzed in detail as illustrated in Figs. 22 and 23.

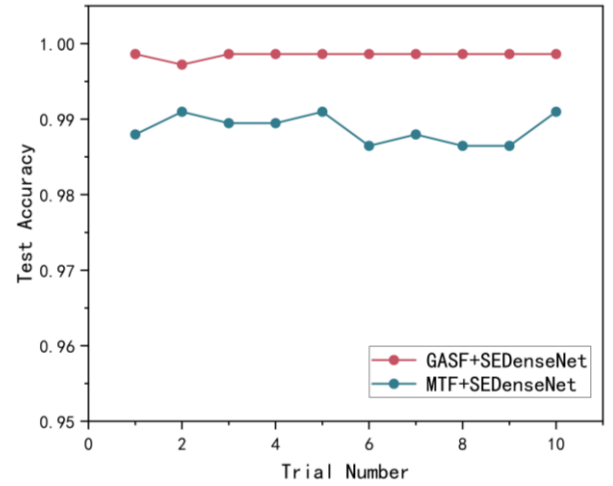
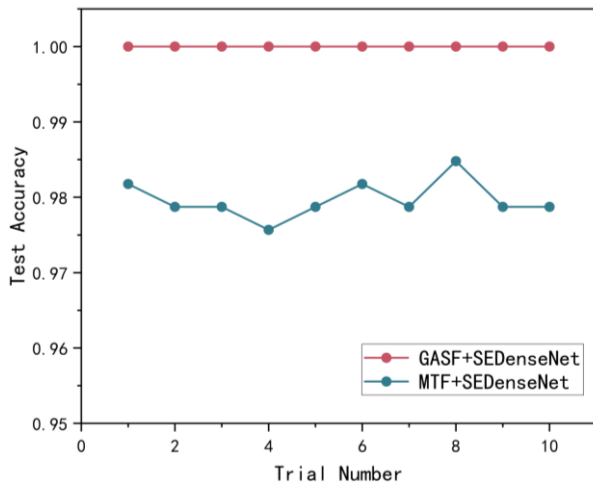


(a) Gearbox data network model comparison



(b) Bearing data network model comparison

Fig. 22. Accuracy of 10 validations of different network models for case 2.



(a) Gearbox data signal preprocessing comparison

(b) Bearing data signal preprocessing comparison

Fig. 23. Accuracy of 10 validations for different signal preprocessing methods in Case 2.

The 10 validation results of the gearbox dataset in Case 2 all achieved 100% diagnostic accuracy, while the 10 validation results of the bearing dataset had 9 diagnostic accuracies of 99.86% and 1 diagnostic accuracy of 99.72%, respectively. This corresponded to 1 incorrect classification in the other categories in the test set for bearings and 2 for gearboxes.

The average accuracy of ten validations of the network model proposed in this paper with the five network models compared and the MTF coding technique is shown in Tables 5,6. Table 5. Comparison of average accuracy of different network models and signal preprocessing methods for gearbox data.

Model	Accuracy(%)
GAF+SEDenseNet	100±0
GAF+DenseNet	99.71±0.09
GAF+ResNet50	99.45±0.13
GAF+EfficientNet	98.72±0.32
GAF+VGG16	98.48±0.29
GAF+ShuffleNet	95.5±0.54
MTF+SEDenseNet	97.96±0.25

Table 6. Comparison of average accuracy of different network models and signal preprocessing methods for bearing data.

Model	Accuracy(%)
GAF+SEDenseNet	99.85±0.04
GAF+DenseNet	99.15±0.28
GAF+ResNet50	98.09±0.18
GAF+EfficientNet	98.75±0.15
GAF+VGG16	97.14±0.36
GAF+ShuffleNet	95.38±0.25
MTF+SEDenseNet	98.87±0.19

## 6. Fault diagnosis model performance metrics

The potential ramifications of failing to identify or accurately report fault types during diagnosis are significant, thus the diagnostic accuracy metric alone cannot be utilized to assess the effectiveness of the fault diagnosis model. To comprehensively evaluate the model's performance, four key indicators will be considered: accuracy, precision, recall, and F1 value.

In the rotating machinery health state classification model proposed in this paper, the true categories of the samples and the model's predicted categories are classified into four distinct groups: True Positive (TP), False Positive (FP), True Negative (TN), and False Negative (FN).

In order to ensure that the fault diagnostic model does not experience false alarms, the performance measure of the model is performed using precision, where the precision formula is as follows:

$$Precision = \frac{TP}{TP+FP} \quad (11)$$

In order to ensure that the fault diagnostic model does not suffer from underreporting, recall is used to measure the performance of the model, where the recall formula is as follows:

$$Recall = \frac{TP}{TP+FN} \quad (12)$$

Given that various types of troubleshooting exhibit varying preferences for model predictions, the F1 score is calculated by taking a reconciled average of precision and recall, using the following formula:

$$F1 = \frac{2 \times Precision \times Recall}{Precision + Recall} \quad (13)$$

The most satisfactory results of the three sets of data were chosen to assess the fault diagnostic model's performance, as Table 7. Model metric average results.

	Case1 bearing data	Case2 gearbox data	Case2 bearing data
Accuracy(%)	100	100	99.861304
Precision(%)	100	100	99.862637
Recall(%)	100	100	99.861304
F1(%)	100	100	99.861301
Support	329	329	721

Receiver operating characteristic (ROC) curve is a comprehensive metric that assesses the sensitivity and specificity of a continuous variable. The points on the ROC curve represent the perceptibility of a given signal stimulus. The ROC curve displays the true positive rate (TPR, sensitivity) on the vertical axis and the false positive rate (FPR, specificity) on the horizontal axis. The ROC curve is as follows:

$$TPR = \frac{TP}{TP+FN} \quad (14)$$

illustrated in Table 7, which displays the average values across ten trials.

$$FPR = \frac{FP}{TP+FP} \quad (15)$$

As the specificity increases, the optimal classification results are obtained when the sensitivity reaches 1. In other words, the larger the area under the seven health state curves is, the better the experimental results will be. The ROC curves for Case 1, as depicted in Fig. 24, demonstrate that the optimal classification results are achieved when the area under each of the ROC curves is equal to 1 for each category.

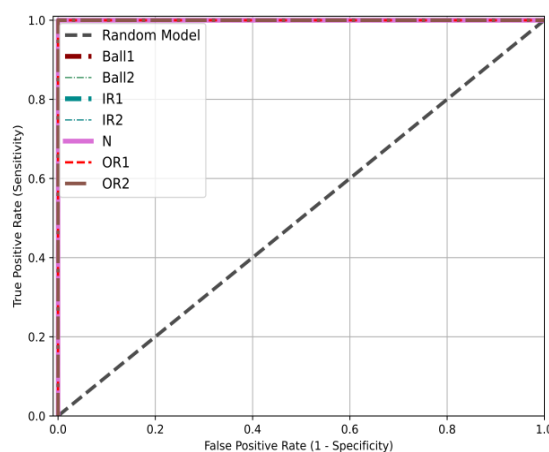


Fig. 24. ROC curve for Case 1 experiment.

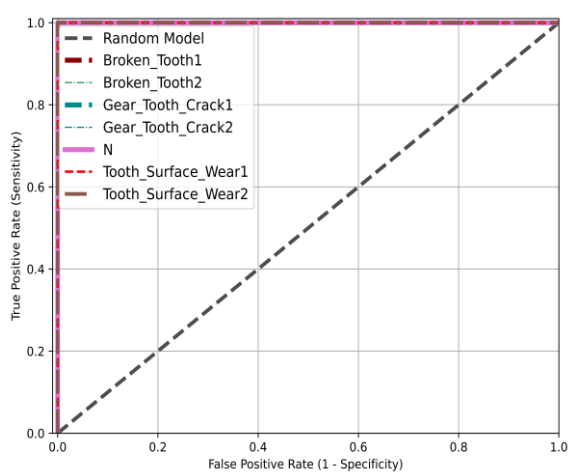


Fig. 25. Case 2 gearbox data experiment ROC curve.

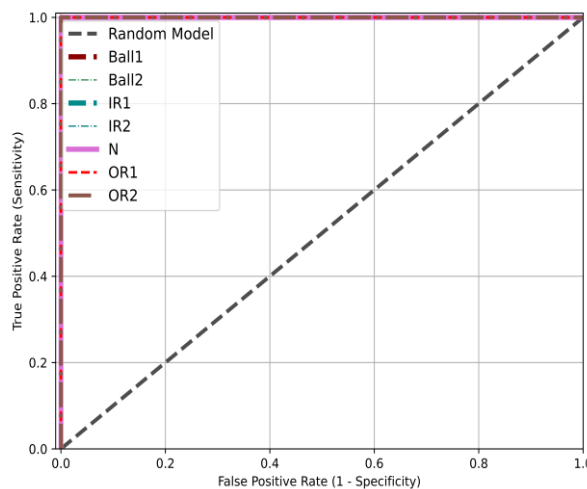


Fig. 26. Case 2 bearing data experiment ROC curve.

As can be observed from the ROC curves of the two types of data in Case 2, the area under each of the ROC curves for the two types of data is almost equal to 1, indicating that the model proposed in this paper achieves outstanding results in classifying the health states of both types of data.

## 7. Conclusions

An intelligent fault diagnosis method for rotating machinery that combines GASF and improved SEDenseNet is proposed in this paper. The effectiveness and superiority of the GASF-SEDenseNet model are verified by utilizing two rolling bearing dataset and one gearbox dataset. The conclusions are as follows:

(1) An GASF coding method is introduced to transform one-dimensional mechanical vibration signals into two-dimensional feature maps. This approach effectively expresses the features in the low-dimensional signals in high-dimensional nonlinear data while preserving the temporal sequence of the original signals. Experimental results demonstrate the superiority of this signal preprocessing method in the field of rotating machinery fault diagnosis.

(2) A novel SEDenseNet fault diagnosis model is proposed, which enhances the transfer and reuse of features through its dense connectivity mechanism. Additionally, the introduction of the SE attention mechanism enables the network to learn feature information and enhances the representation of informative features. Compared to traditional densely connected networks, SEDenseNet avoids network degradation and accelerates the training process.

(3) The proposed fault diagnosis method is validated using

the CWRU dataset with bearings and gearboxes under different operating conditions in the WTDS dataset. The results demonstrate that compared to other deep learning methods, the GASF-SEDenseNet model achieves the highest accuracy on the test set, with Precision, Recall, and F1 values above 99.86%, which represents the best overall performance. Furthermore, the results of confusion matrix and t-SNE visualization reveal that GASF-SEDenseNet has strong feature mining capabilities and can effectively classify the health status of rotating machinery.

This study focuses on deep neural network structures tailored specifically for fault diagnosis in rotating machinery, a methodology aimed at significantly enhancing both the accuracy and robustness of fault diagnosis. However, the proposed method also exhibits certain limitations. Notably, it necessitates the prior monitoring of common fault types and the training of corresponding fault data. Failure to do so may result in misclassification of unlearned fault types into trained categories. Additionally, the method relies solely on a single vibration signal and has yet to incorporate the fusion of multiple data sources for fault diagnosis. Moreover, it demands a substantial amount of pre-collected data to yield satisfactory results. In subsequent work, it is expected that federated transfer learning will be employed to address these constraints, aiming to acquire a more comprehensive dataset that includes a variety of faults observed in industrial rotating machinery. Furthermore, the future work will involve the multimodal fusion of other signals with vibration data to further improve and optimize the proposed fault diagnosis method.

## References

1. Liu S, Ji Z, Wang Y, Zhang Z, Xu Z, Kan C, et al. Multi-feature fusion for fault diagnosis of rotating machinery based on convolutional neural network. *Computer Communications*. 2021;173:160-9. <https://doi.org/10.1016/j.comcom.2021.04.016>
2. Cen J, Yang ZH, Liu X, Xiong JB, Chen HH. A Review of Data-Driven Machinery Fault Diagnosis Using Machine Learning Algorithms. *JOURNAL OF VIBRATION ENGINEERING & TECHNOLOGIES*. 2022;10(7):2481-507. <https://doi.org/10.1007/s42417-022-00498-9>
3. Lei Y, Yang B, Jiang X, Jia F, Li N, Nandi AK. Applications of machine learning to machine fault diagnosis: A review and roadmap. *Mechanical Systems and Signal Processing*. 2020;138. <https://doi.org/10.1016/j.ymssp.2019.106587>
4. Chen X, Yang R, Xue Y, Huang M, Ferrero R, Wang Z. Deep Transfer Learning for Bearing Fault Diagnosis: A Systematic Review Since 2016. *IEEE Transactions on Instrumentation and Measurement*. 2023;72:1-21. <https://doi.org/10.1109/TIM.2023.3244237>
5. Ye M, Yan X, Jia M. Rolling Bearing Fault Diagnosis Based on VMD-MPE and PSO-SVM. *Entropy*. 2021;23(6). <https://doi.org/10.3390/e23060762>
6. Liu X, Tang B, Li Q, Yang Q. Twin prototype networks with noisy label self-correction for fault diagnosis of wind turbine gearboxes. *Measurement Science and Technology*. 2022;34(3):035006. <https://doi.org/10.1088/1361-6501/aca3c3>
7. Guo J, Si Z, Xiang J. Cycle kurtosis entropy guided symplectic geometry mode decomposition for detecting faults in rotating machinery.

- ISA Transactions. 2023;138:546-61. <https://doi.org/10.1016/j.isatra.2023.03.026>
8. Su Z, Wang F, Xiao H, Yu H, Dong S. A fault diagnosis model based on singular value manifold features, optimized SVMs and multi-sensor information fusion. *Measurement Science and Technology*. 2020;31(9):095002. <https://doi.org/10.1088/1361-6501/ab842f>
  9. Li T, Peng Z, Xu H, He Q. Parameterized Domain Mapping for Order Tracking of Rotating Machinery. *IEEE Transactions on Industrial Electronics*. 2023;70(7):7406-16. <https://doi.org/10.1109/TIE.2022.3201311>
  10. Li S, Li T, Sun C, Chen X, Yan R. WPCovNet: An Interpretable Wavelet Packet Kernel-Constrained Convolutional Network for Noise-Robust Fault Diagnosis. *IEEE Transactions on Neural Networks and Learning Systems*. 2023;1-15. <https://doi.org/10.1109/TNNLS.2023.3282599>
  11. Aasi A, Tabatabaei R, Aasi E, Jafari SM. Experimental investigation on time-domain features in the diagnosis of rolling element bearings by acoustic emission. *Journal of Vibration and Control*. 2021;28(19-20):2585-95. doi: 0.1177/10775463211016130
  12. Zhou Y, Sun W, Ye C, Peng B, Fang X, Lin C et al. Time-frequency Representation -enhanced Transfer Learning for Tool Condition Monitoring during milling of Inconel 718. *Eksploracja i Niezawodność – Maintenance and Reliability*. 2023;25(2). <https://doi.org/10.17531/ein/165926>
  13. Lei Y, Jia F, Lin J, Xing S, Ding SX. An Intelligent Fault Diagnosis Method Using Unsupervised Feature Learning Towards Mechanical Big Data. *IEEE Transactions on Industrial Electronics*. 2016;63(5):3137-47. <https://doi.org/10.1109/TIE.2016.2519325>
  14. Zhang C, Zhang L. Wind turbine pitch bearing fault detection with Bayesian augmented temporal convolutional networks. *Structural Health Monitoring*. 2023. <https://doi.org/10.1177/14759217231175886>
  15. Wang Q, Xu F. A novel rolling bearing fault diagnosis method based on Adaptive Denoising Convolutional Neural Network under noise background. *Measurement*. 2023;218. <https://doi.org/10.1016/j.measurement.2023.113209>
  16. Wang H, Sun W, He L, Zhou J. Intelligent Fault Diagnosis Method for Gear Transmission Systems Based on Improved Multi-Scale Reverse Dispersion Entropy and Swarm Decomposition. *IEEE Transactions on Instrumentation and Measurement*. 2022;71:1-13. <https://doi.org/10.1109/TIM.2021.3115207>
  17. Chen T, Zhang X, Wang C, Yu X, Wang S, Chen X. Domain adversarial neural network-based nonlinear system identification for helicopter transmission system. *Nonlinear Dynamics*. 2023;111(16):14695-711. <https://doi.org/10.1007/s11071-023-08657-7>
  18. Cheng Y, Lin M, Wu J, Zhu H, Shao X. Intelligent fault diagnosis of rotating machinery based on continuous wavelet transform-local binary convolutional neural network. *Knowledge-Based Systems*. 2021;216. <https://doi.org/10.1016/j.knsys.2021.106796>
  19. Wang X, Mao D, Li X. Bearing fault diagnosis based on vibro-acoustic data fusion and 1D-CNN network. *Measurement*. 2021;173. <https://doi.org/10.1016/j.measurement.2020.108518>
  20. Luo P, Yin Z, Yuan D, Gao F, Liu J. An Intelligent Method for Early Motor Bearing Fault Diagnosis Based on Wasserstein Distance Generative Adversarial Networks Meta Learning. *IEEE Transactions on Instrumentation and Measurement*. 2023;72:1-11. <https://doi.org/10.1109/TIM.2023.3278289>
  21. Xia M, Li T, Xu L, Liu L, de Silva CW. Fault Diagnosis for Rotating Machinery Using Multiple Sensors and Convolutional Neural Networks. *IEEE/ASME Transactions on Mechatronics*. 2018;23(1):101-10. <https://doi.org/10.1109/TMECH.2017.2728371>
  22. Chen Z, Mauricio A, Li W, Gryllias K. A deep learning method for bearing fault diagnosis based on Cyclic Spectral Coherence and Convolutional Neural Networks. *Mechanical Systems and Signal Processing*. 2020;140. <https://doi.org/10.1016/j.ymssp.2020.106683>
  23. Xiong J, Li C, Wang C-D, Cen J, Wang Q, Wang S. Application of Convolutional Neural Network and Data Preprocessing by Mutual Dimensionless and Similar Gram Matrix in Fault Diagnosis. *IEEE Transactions on Industrial Informatics*. 2022;18(2):1061-71. <https://doi.org/10.1109/TII.2021.3073755>
  24. Bai Y, Yang J, Wang J, Zhao Y, Li Q. Image representation of vibration signals and its application in intelligent compound fault diagnosis in railway vehicle wheelset-axlebox assemblies. *Mechanical Systems and Signal Processing*. 2021;152. <https://doi.org/10.1016/j.ymssp.2020.107421>
  25. He D, Lao Z, Jin Z, He C, Shan S, Miao J. Train bearing fault diagnosis based on multi-sensor data fusion and dual-scale residual network. *Nonlinear Dynamics*. 2023;111(16):14901-24. <https://doi.org/10.1007/s11071-023-08638-w>
  26. Fan C, Lin Y, Piscitelli MS, Chiosa R, Wang H, Capozzoli A, et al. Leveraging graph convolutional networks for semi-supervised fault diagnosis of HVAC systems in data-scarce contexts. *Building Simulation*. 2023;16(8):1499-517. <https://doi.org/10.1007/s1227302310411>

27. Chang C, Wang Q, Jiang J, Jiang Y, Wu T. Voltage fault diagnosis of a power battery based on wavelet time-frequency diagram. *Energy*. 2023;278. <https://doi.org/10.1016/j.energy.2023.127920>
28. Wang, X., Yao, Y., and Gao, C. (2024). Wasserstein Distance- EEMD Enhanced Multi-Head Graph Attention Network for Rolling Bearing Fault Diagnosis Under Different Working Conditions. *Eksploatacja i Niezawodność – Maintenance and Reliability*. <https://doi.org/10.17531/ein/184037>
29. Tong J, Liu C, Zheng J, Pan H. Multi-sensor information fusion and coordinate attention-based fault diagnosis method and its interpretability research. *Engineering Applications of Artificial Intelligence*. 2023;124. <https://doi.org/10.1016/j.engappai.2023.106614>
30. Xia S, Zhou X, Shi H, Li S, Xu C. A fault diagnosis method with multi-source data fusion based on hierarchical attention for AUV. *Ocean Engineering*. 2022;266. <https://doi.org/10.1016/j.oceaneng.2022.112595>
31. Wang Z, Oates T. Imaging time-series to improve classification and imputation. *arXiv preprint arXiv:150600327*. 2015. <https://doi.org/10.48550/arXiv.1506.00327>
32. Keogh EJ, Pazzani MJ, editors. Scaling up dynamic time warping for datamining applications. *Proceedings of the sixth ACM SIGKDD international conference on Knowledge discovery and data mining*; 2000. <https://doi.org/10.1145/347090.347153>
33. Huang G, Liu Z, Van Der Maaten L, Weinberger KQ. Densely Connected Convolutional Networks. 2017 IEEE Conference on Computer Vision and Pattern Recognition (CVPR)2017. p. 2261-9. <https://doi.org/10.1109/CVPR.2017.243>
34. Hu J, Shen L, Sun G. Squeeze-and-Excitation Networks. 2018 IEEE/CVF Conference on Computer Vision and Pattern Recognition2018. p. 7132-41. <https://doi.org/10.1109/CVPR.2018.00745>
35. Smith WA, Randall RB. Rolling element bearing diagnostics using the Case Western Reserve University data: A benchmark study. *Mechanical systems and signal processing*. 2015;64:100-31. <https://doi.org/10.1016/J.YMSSP.2015.04.021>